RSC Advances

PAPER

View Article Online
View Journal | View Issue

Cite this: *RSC Adv.*, 2023, **13**, 7682

Optimization of a polyvinyl butyral synthesis process based on response surface methodology and artificial neural network†

Wenwen Luan, Li Sun, Zuoxiang Zeng * and Weilan Xue

High quality polyvinyl butyral (PVB) can be used as the intermediate film of automobile and building glass and the packaging film of photovoltaic cells. Therefore, it is necessary to optimize its synthesis process to obtain suitable products with a high acetalization degree (AD) and small particle size (d_p). In this work, a deep eutectic solvent (DES) was selected as the catalyst, and response surface methodology (RSM) and artificial neural network (ANN) were utilized to optimize the synthesis process of PVB. The concentration of polyvinyl alcohol (*A*), the dosage of DES (*B*) and *n*-butanal (*C*), and the aging temperature (*D*) were selected as process variables, and the comprehensive score (AD, d_p and material and energy consumption) was introduced as the response. The results showed that single-factors *B*, *C*, *D*, and the interactions *AB*, *BC* and *CD* had significant effects on the comprehensive score, and the qualified PVB products (AD > 81%, d_p = 3–3.5 μm) were obtained under the optimal conditions obtained by RSM and ANN models. ANN is a better and more precise optimization tool than RSM. Also, DES played a dual role in catalysis and dispersion in the synthesis of PVB and showed good reusability, so it has great application potential in PVB industrial production.

Received 19th December 2022
Accepted 26th February 2023

DOI: 10.1039/d2ra08099k

rsc.li/rsc-advances

1. Introduction

Polyvinyl butyral (PVB) is an important synthetic resin, which has the advantages of strong adhesion, great flexibility, high UV stability and optical transparency, and excellent impact and weather resistance.[1–3] PVB is usually used as interlayer material for laminated glass in automobiles and buildings, due to its strong adhesion to glass, excellent mechanical strength, and optical clarity.[4–6] Recently, PVB has gained wide attention because of its great potential for applications in encapsulation film for solar cells,[7,8] protective coating for metal substrates,[9–11] and ultrafiltration membrane for wastewater treatment.[12–14]

The acetalization degree (AD) of PVB is one of the most important parameters determining its application performance such as mechanical and thermal properties, bond strength and water resistance. To meet the mechanical and hydrophobic property requirements for application, the AD value needs to reach more than 78%.[3] In addition, the particle size (d_p) is also an important parameter for PVB application, and it is closely related to the purity, acetalization degree, and intermolecular crosslinking of PVB products, all of which are strictly required in ultrafiltration membranes, biomedical applications and photovoltaic cells.[15] The performance of PVB depends mainly on its synthesis process, which involves the acetal reaction of polyvinyl alcohol (PVA) and *n*-butanal (BA) in the presence of an acidic catalyst. Therefore, to meet the extreme demand of some applications, the synthesis process of PVB becomes important to produce high quality PVB products with high AD value, and small and uniform particle sizes.

PVB resin is mainly produced by the precipitation method in the industry, which involves two temperature-controlled stages: the condensation stage (reaction at a low temperature) and the aging stage (reaction at a high temperature).[3,16] Precipitation method is relatively mature, but there are still disadvantages such as low degree of acetalization, easy agglomeration and high energy consumption. In recent years, researchers have been working to improve the PVB synthesis process by changing the solvent system, improving the reaction device and using new catalysts. Fernández *et al.*[17] used *N*-methylpyrrolidone (NMP) instead of water as a reaction medium to prepare PVB, and products with different degrees of acetalization were prepared in a homogeneous system. But this method requires special solvents, and the separation and purification of the product from the solvent are difficult. Lin *et al.*[16] and Zhou *et al.*[3] used membrane dispersion microreactors to synthesize PVB, which had a strong mixing capacity, shortened reaction time and reduced energy consumption. However, the production cost of the microreactor is high, and PVB particles are easy to block the channels, so it is difficult to industrially produce PVB with the microreactor. Typically, a strong inorganic acid (usually HCl or H_2SO_4) is used as the catalyst for PVB synthesis,

School of Chemical Engineering, East China University of Science and Technology, 200237 Shanghai, China. E-mail: zengzx@ecust.edu.cn

† Electronic supplementary information (ESI) available. See DOI: https://doi.org/10.1039/d2ra08099k

which has the disadvantages of corrosion of equipment, agglomeration of PVB particles and uneven distribution of acetalization degree. Researchers today are trying to develop new catalysts to replace inorganic acids. In recent years, ionic liquids (ILs) have become increasingly attractive as novel and efficient catalysts because of their low vapor pressure, non-flammability, and excellent chemical and thermal stability.[18–20] Qin *et al.*[21] successfully synthesized PVB using *N*-methylimidazole sulfate ($[HMIM]^+HSO_4^-$) as an IL catalyst, and the AD value of the product was up to 72%. Nevertheless, ILs are expensive and difficult to biodegrade.[22] Deep eutectic solvent (DES) has been developed as a novel alternative to ILs.[23,24] It is synthesized by mixing a hydrogen bond acceptor (HBA) (quaternary ammonium salts) and a hydrogen bond donor (HBD) (carboxylic acids) at 60–80 °C,[25–27] and is cheap, biodegradable, low toxic and reusable.[28–30] Hence, DES as a catalyst has potential applications in polymer chemistry and synthetic organic chemistry.

Traditionally, surfactants are added to the reaction system to disperse reactants and product molecules during PVB synthesis, thus improving particle aggregation. However, too much surfactant residue in PVB will cause it to turn yellow during high temperature processing.[31] Fortunately, DES also has good dispersal ability and is widely used as an efficient dispersant for the chemical synthesis of advanced nanomaterials.[32–34] Therefore, DES is expected to achieve a double goal of catalysis and dispersion in the synthesis of PVB. Furthermore, DES has excellent reusability performance, which is an important factor for the possibility of its use in large-scale industrial applications.

Response surface methodology (RSM) is a powerful tool for optimizing process conditions.[35–37] The Box–Behnken design (BBD), a type of RSM design, can provide 3–7 factors and three levels of experimental conditions. BBD has proven to be more efficient than the other response surface designs and has been widely used in the field of chemical engineering due to its benefits such as fewer experiments, shorter time and lower costs.[38,39] Rathee *et al.*[40] optimized the prepared phytosomes formulations using a 3-factor, 3-level BBD, and the results showed that the polyherbal phytosome preparation can be used as an alternative to dosage form design and delivery.

Artificial neural network (ANN) is a powerful data processing technology based on mimicking the biological nervous systems. Because of its advantages of mega-parallelism, high nonlinearity, self-learning, tolerance to scattered data and fast processing speed,[41,42] ANN has been widely applied in many fields such as prediction,[43] classification,[44] signal processing,[45,46] image processing[47,48] and chemical process control.[49–51] ANN trains experimental data by establishing relationships between input and output variables to predict and optimize complex processes.[52,53] Haido[54] established new empirical ANN models to evaluate the performance of RC connections based on a database of more than 200 experiments from the literature. The results showed that the obtained ANN models are stable and simple, and are suitable for the expected beam–column joint structure design.

RSM modeling consists of two steps, *i.e.*, designing experiments and establishing a model based on the experimental results. ANN can derive models from available data without prior design or adjustment.[55] Their features help to compare the models obtained by RSM and ANN and to combine the advantages of both methods to better solve complex problems.[56,57] Toppo *et al.*[57] used RSM and ANN models to optimize the synthesis process conditions of gold nanoparticles. The experiments were designed by RSM and the obtained model was further optimized by ANN. Ezemagu *et al.*[56] optimized the process conditions for turbidity removal from produced water using RSM and ANN techniques.

In this study, DES formed by benzyltrimethylammonium chloride (BAC) and *p*-toluene sulphonic acid (PTSA) was selected as the catalyst for the synthesis of PVB, and the process conditions were optimized using both RSM and ANN. The four factors considered in this work are as follows: PVA concentration (w_{PVA}), DES dosage (m_{DES}/m_{PVA}), *n*-butanal dosage (m_{BA}/m_{PVA}) and aging temperature (T_{age}). The comprehensive score considering acetalization degree, particle size and energy consumption was introduced as the response. Validation experiments were carried out to confirm the efficacy of RSM and ANN models, and their prediction accuracy was compared. Finally, recycling experiments were carried out to examine the reusability of DES.

2. Materials and methods

2.1 Materials

PVA (MW 24 000–24 500 g mol^{-1}, hydrolysis degree of 99.0%) and ethanol (99.5%) were supplied by Shanghai Macklin Biochemical Co., Ltd. *n*-Butanal (99.5%) was got from Shanghai Mairuier Chemical Technology Co., Ltd. Benzyltrimethylammonium chloride (BAC, 98.0%) was got from Shanghai Di Bo Chemical Co., Ltd. *p*-Toluenesulfonic acid monohydrate (PTSA, 99.0%) was got from Shanghai Aladdin Biochemical Technology Co., Ltd. Sodium dodecyl sulfonate (SDS, 97.0%) and sodium hydroxide (NaOH, 98.0%) was supplied by Sinopharm Chemical Reagent Co., Ltd. Hydrochloric acid (HCl, 36–38%) and hydroxylamine hydrochloride (98.5%) were bought from Shanghai Titan Scientific Co., Ltd.

2.2 Synthesis of PVB

The detailed reaction mechanism of PVB synthesis is shown in Fig. 1, and it is described as follows. First, *n*-butanal is protonated under acidic conditions, and the protonated *n*-butanal then reacts with the hydroxyl group on the PVA molecule to form a protonated hemiacetal group. Next, the protonated hemiacetal loses one H_2O molecule and reacts with the neighboring hydroxyl group to form an acetal group. Finally, H^+ leaves and the acetal reaction is complete.[58] The synthetic procedure of PVB is similar to that of our previous publication,[59] and it is described in detail in ESI.†

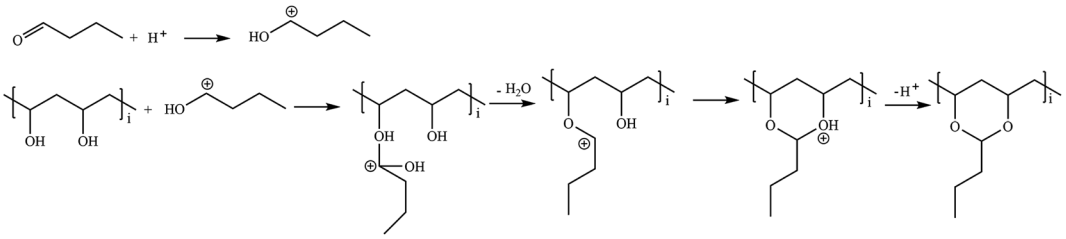

Fig. 1 Reaction mechanism of PVB synthesis.

2.3 Preparation and selection of DES

The preparation procedure of DES has been described in detail in our previous study,[58] and it can be found in ESI.† Experiments of selecting catalyst were carried out, and results showed that DES (BAC–PTSA) prepared by BAC and PTSA with a molar ratio of 1 exhibited the best catalysis effect for PVB synthesis. The detailed results and the characterization of DES are shown in ESI.†

2.4 Evaluation of the catalytic performance of DES

To evaluate the catalytic performance of DES, BAC–PTSA and HCl were used as the catalyst to synthesize PVB, and the dosage of the catalyst was determined by the pH of the system (adjusted to ~1.5). For these two catalysts, the dosage of SDS (m_{SDS}/m_{PVA}) is 0.01 and 0.03, respectively, and the samples obtained are named PVB–DES and PVB–HCl, respectively. The AD values of the samples were determined to be almost identical (~80%). The SEM images of the two samples are shown in Fig. 2. Interestingly, despite the much lower amount of surfactant, PVB products with the smaller particle size were obtained with the presence of DES. Specifically, the d_p was measured to be ~6.6 μm (PVB–HCl) and ~4.2 μm (PVB–DES) respectively. The results indicated that DES played a dual role in catalysis and dispersion in the synthesis of PVB, and it was selected as the catalyst to synthesize PVB in this study.

2.5 Determination of acetalization degree of PVB

The AD value of PVB is determined by the hydroxylamine hydrochloride method,[59,60] which is defined as the mass ratio of acetal groups to the total mass of the molecular chain, and it can be calculated by eqn (1):

$$AD(\%) = \frac{0.142 \times (V - V_0) \times C}{m} \times 100 \quad (1)$$

where V and V_0 (mL) are the volumes of NaOH solution consumed by PVB and the blank group, respectively; C (mol L^{-1}) is the concentration of NaOH solution; m (g) is the amount of PVB sample, and 0.142 is a constant related to the molecular weight of an acetal unit.

2.6 Characterization of PVB

The samples of PVA and PVB were characterized by Fourier transition infrared spectroscopy (FTIR, Thermo Fisher Scientific Nicolet iS10, USA) on the specimens made through KBr. The glass transition temperature (T_g) was measured by a differential scanning calorimeter (DSC1, Mettler Toledo Switzerland) under a nitrogen atmosphere. Thermogravimetric analysis (TGA, NETZSCH STA 449F5 simultaneous thermal analyzer) was utilized to measure the thermal stability of PVB products, and the test was carried out at a heating rate of 10 °C min^{-1} from 25 °C to 700 °C under an air atmosphere. Gel permeation chromatography (GPC, Waters 1515, USA) was used to determine the molecular weight of PVB, and the values were calculated by the calibration curve of polystyrene standards. A scanning electron microscope (SEM, S-3400N, Hitachi) was utilized to image PVB particles and measure the particle size. UV spectrophotometer (UV-1800, Shimadzu) was used to determine the concentration of *n*-butanal.

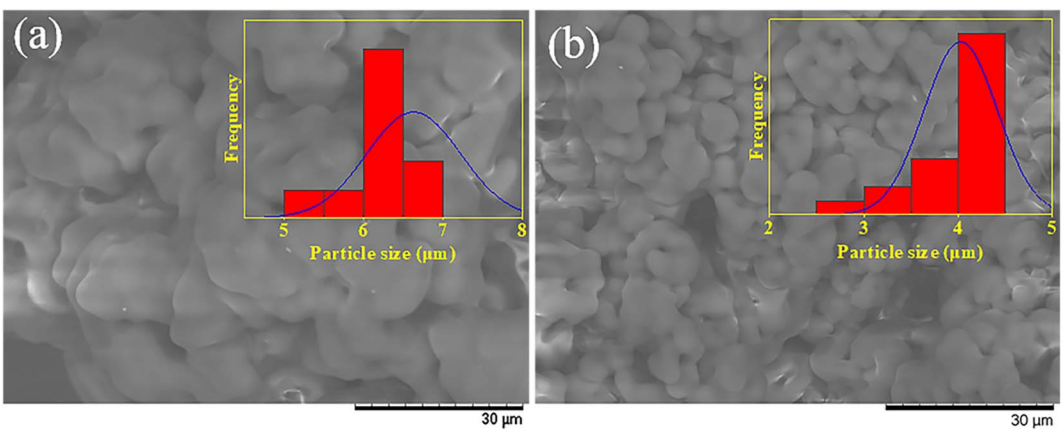

Fig. 2 SEM images of PVB samples: (a) PVB–HCl and (b) PVB–DES.

Table 1 The codes of four factors and their three levels

	Factors	Unit	Coded and actual levels		
			−1	0	+1
A	w_{PVA}	%	4	7	10
B	m_{DES}/m_{PVA}	g g^{-1}	0.1	0.2	0.3
C	m_{BA}/m_{PVA}	g g^{-1}	0.60	0.75	0.90
D	T_{age}	°C	50	60	70

2.7 RSM modeling

2.7.1 Determination of the range of four factors in the RSM design. Before the RSM experiments, single-factor experiments were carried out to investigate the effects of four factors (w_{PVA}, m_{DES}/m_{PVA}, m_{DES}/m_{PVA}, T_{age}) on the reaction. Based on this, the variation range of them in the RSM experiment design was determined as follows:

(1) PVA concentration (w_{PVA}): when the w_{PVA} value is too high (>10%), the molecular chains of PVA cannot stretch freely, which is unfavorable to the reaction of hydroxyl groups with *n*-butanal. However, too small w_{PVA} value (<4%) leads to too low equipment utilization. Therefore, the suitable range of w_{PVA} is 4–10%.

(2) DES dosage (m_{DES}/m_{PVA}): if the catalyst dosage is lower than 0.1, the reaction rate would be very slow. When the value of m_{DES}/m_{PVA} is higher than 0.3, the concentration of protonated *n*-butanal will reach the threshold value, and the reaction rate no longer increases with increasing DES dosage. Therefore, the suitable range of m_{DES}/m_{PVA} is 0.1–0.3.

(3) *n*-Butanal dosage (m_{BA}/m_{PVA}): the AD value of PVB increases with the increase of m_{BA}/m_{PVA} until m_{BA}/m_{PVA} is 0.9, and then tends to be stable. On the other hand, when m_{BA}/m_{PVA} < 0.6, the reaction rate is too low. So, the suitable range of m_{BA}/m_{PVA} is 0.6–0.9.

(4) Aging temperature (T_{age}): if T_{age} is lower than 50 °C, the AD value will be lower than 76%; however, when T_{age} > 70 °C, the d_p value of the product will increase significantly. So, the suitable range of T_{age} is 50–70 °C.

The above four factors were selected as input variables in RSM and each variable was set at three levels: low (−1), medium (0), and high (+1) as shown in Table 1.

2.7.2 Indicators for evaluating experimental results. In this work, RSM and ANN were used to optimize the synthesis process conditions of PVB, and the experimental results were evaluated by the comprehensive score which includes the AD value of PVB (weight 70%), the d_p value of PVB (weight 20%) and material and energy consumption (weight 10%). The formula for calculating the comprehensive score (Y) is as follows:

$$Y = \left(0.7 \times \frac{AD_i}{AD_{max}} + 0.2 \times \frac{(d_p)_{min}}{(d_p)_i} + 0.1 \times \frac{E_{min}}{E_i}\right) \times 100 \quad (2)$$

where AD_{max} is the maximum value of AD, $(d_p)_{min}$ is the minimum value of particle size and E_{min} is the minimum value of material and energy consumption.

Table 2 Experimental design and results of RSM

Run	Factors and coded levels				Comprehensive score
	A (%)	*B* (g g^{-1})	*C* (g g^{-1})	*D* (°C)	
1	0	0	−1	1	76.87
2	−1	0	0	−1	89.61
3	0	0	0	0	90.80
4	0	−1	1	0	81.05
5	0	0	1	−1	86.10
6	0	−1	0	−1	87.32
7	1	0	1	0	84.69
8	0	0	−1	−1	87.70
9	1	0	0	−1	87.61
10	0	1	−1	0	81.70
11	0	1	0	1	83.59
12	0	−1	−1	0	82.17
13	0	1	1	0	87.52
14	0	0	0	0	91.01
15	1	−1	0	0	84.16
16	0	0	0	0	91.49
17	1	1	0	0	85.85
18	−1	0	−1	0	79.87
19	0	0	0	0	91.09
20	0	−1	0	1	79.89
21	−1	−1	0	0	81.32
22	−1	0	0	1	81.85
23	0	0	1	1	83.95
24	−1	1	0	0	88.55
25	0	0	0	0	91.59
26	1	0	0	1	80.93
27	0	1	0	−1	90.26
28	−1	0	1	0	85.65
29	1	0	−1	0	81.70

2.7.3 RSM experimental design. Twenty-nine experimental runs designed by RSM based on a four-factor-three-level BBD are shown in Table 2. A quadratic polynomial equation was used to analyze the relationship between the response and independent variables as follows:

$$Y = \beta_0 + \beta_1 A + \beta_2 B + \beta_3 C + \beta_4 D + \beta_{11} A^2 + \beta_{22} B^2 + \beta_{33} C^2 + \beta_{44} D^2 + \beta_{12} AB + \beta_{13} AC + \beta_{14} AD + \beta_{23} BC + \beta_{24} BD + \beta_{34} CD \quad (3)$$

where Y is the response variable (comprehensive score), and A, B, C and D are the process factors in the model. β_0 is the constant coefficient; β_1, β_2, β_3 and β_4 are the main coefficient that determines the effect of factors on the response; β_{11}, β_{22}, β_{33} and β_{44} are the quadratic coefficients; β_{12}, β_{13}, β_{14}, β_{23}, β_{24} and β_{34} are the interactive coefficients between different factors.

2.8 ANN modeling

In ANN, a back propagation (BP) was used, which is a multilayer feedforward neural network trained by the error back-propagation learning algorithm and has strong stability. The basic structure of the BP ANN model consists of input, hidden, and output layers, and the node of each layer in the ANN model was determined as follows.

(1) Input layer: the input layer includes four variables that affect the quality of PVB product: PVA concentration, DES dosage, *n*-butanal dosage and aging temperature.

(2) Output layer: the output layer includes one node, which is the comprehensive score as an evaluation indicator.

(3) Hidden layer: the number of hidden layer nodes can directly affect the performance of the ANN model. The determination of hidden layer nodes includes two steps. First, a reasonable range of the number of nodes in the hidden layer is inferred using an empirical formula. Then the number of nodes was increased from small to large, and the trial-and-error approach was used to finally determine the optimal number. One common empirical formula is shown in eqn (4):[61]

$$r = 2n + 1 \tag{4}$$

where r is the number of nodes in the hidden layer and n is the number of input nodes.

In this study, Levenberg–Marquardt was selected as the training algorithm because of its fast convergence speed. The mean squared error (MSE) and the correlation coefficient (R^2) were used to estimate the performance of the network. The ANN model and related parameter variations are determined based on the minimum of the MSE. The data obtained from the RSM design will be used to constitute the architecture of ANN and randomly divided into three subsets: 70% for training, 15% for validation and 15% for testing. The maximum number of training epochs is set to 1000 and the final error is less than 0.0001.

2.9 Assessing fit and accuracy of RSM and ANN models

The prediction accuracy of ANN and RSM models can be evaluated by comparing the predicted responses with the experimental responses. Correlation coefficient (R^2), root mean square error (RMSE) and absolute average deviation (AAD%) were often used to determine the accuracy of the models as follows:[62–64]

$$R^2 = \frac{\left(\sum_{i=1}^{N}\left(Y_{i,\mathrm{exp}} - \overline{Y}_{i,\mathrm{exp}}\right)\left(Y_{i,\mathrm{pred}} - \overline{Y}_{i,\mathrm{pred}}\right)\right)^2}{\sum_{i=1}^{N}\left(Y_{i,\mathrm{exp}} - \overline{Y}_{i,\mathrm{exp}}\right)^2\left(Y_{i,\mathrm{pred}} - \overline{Y}_{i,\mathrm{pred}}\right)^2} \tag{5}$$

$$\mathrm{RMSE} = \left(\frac{1}{N}\sum_{i=1}^{N}\left(Y_{i,\mathrm{pred}} - Y_{i,\mathrm{exp}}\right)^2\right)^{\frac{1}{2}} \tag{6}$$

$$\mathrm{AAD\%} = \frac{1}{N}\left(\sum_{i=1}^{N}\frac{\left|Y_{i,\mathrm{exp}} - Y_{i,\mathrm{pred}}\right|}{Y_{i,\mathrm{exp}}}\right) \times 100\% \tag{7}$$

where N is the number of experimental points, $Y_{i,\mathrm{exp}}$, $Y_{i,\mathrm{pred}}$, $\overline{Y}_{i,\mathrm{exp}}$, $\overline{Y}_{i,\mathrm{pred}}$ are the experimental values, predicted values, average experimental values, and average predicted values, respectively.

3. Results and discussion

3.1 Characterization of PVB

3.1.1 FTIR. The FTIR spectra of PVB and PVA are shown in Fig. 3a. As seen in the spectra of PVB, there is a relatively wide

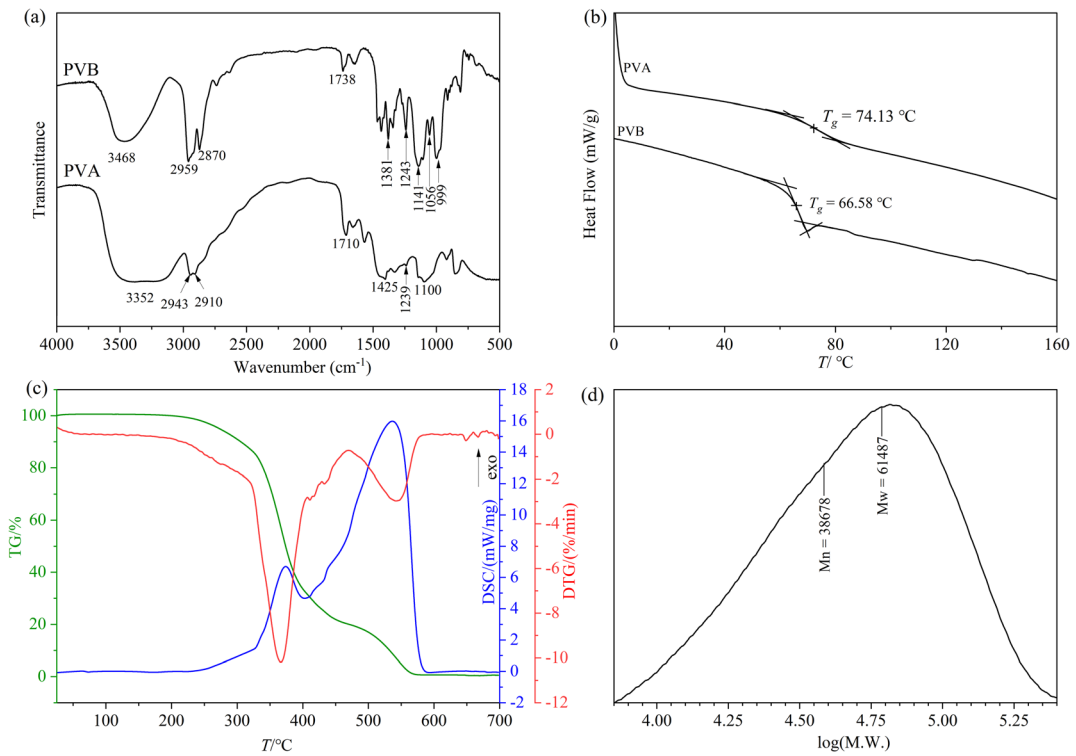

Fig. 3 Characterization of PVB (PVB sample obtained in run 3rd): (a) FTIR spectra of PVA and PVB; (b) the DSC curves of PVA and PVB; (c) TGA -DTG -DSC curves of PVB; (d) GPC profile of PVB.

peak appearing at 3468 cm^{-1}, as a result of –OH stretching.[15] The peak is much weaker than that of PVA, indicating that a large amount of –OH participated in the acetal reaction. The two peaks at 2959 cm^{-1} and 2870 cm^{-1} are assigned to the stretching vibration of C–H. Both PVB and PVA have a small peak at about 1738 cm^{-1}, which is the stretching vibration of C=O of vinyl acetate groups. The peak at 1381 cm^{-1} belongs to the bending vibration of C–H.[21] The two peaks around 1243 cm^{-1} and 1056 cm^{-1} are assigned to the asymmetric and symmetric stretching vibration of the C–O–C of the acetate groups, respectively. The two peaks at 1141 cm^{-1} and 999 cm^{-1} belong to the asymmetric and symmetric stretching vibration of C–O–C–O–C,[65] respectively, which are not found in the spectrum of PVA, confirming that the acetal reaction of PVA and *n*-butanal did occur.

3.1.2 DSC. DSC curves of PVB and PVA are shown in Fig. 3b. From Fig. 3b, it can be seen that the glass transition temperature (T_g) of PVB (66.58 °C) is different from that of PVA (74.13 °C), which is because the regular arrangement of hydroxyl groups in PVA is changed by the introduced butyral group, and the molecular structure and crystallinity of the resulting PVB are also changed.

3.1.3 TGA. TGA was used to measure the thermal stability of PVB products. TG, derivative thermogravimetric (DTG) and DSC curves are shown in Fig. 3c. The temperatures at about 1.5%, 10%, 50% and 90% weight loss are 239 °C, 281 °C, 363 °C and 565 °C, respectively, which represent the thermal stability of the PVB sample. It can be seen from Fig. 3c that in air, due to the generation of oxidation products such as peroxides and carbonyl compounds, there are obvious exothermic peaks on the DSC curve. According to the literature,[66–68] the possible thermal degradation process of PVB in air is described as follows: the first process between 200–380 °C is dominated by oxidation, and the DSC curve shows obvious exothermic phenomenon. There is a small endothermic peak between 400–450 °C, which may be due to the pyrolysis of oxidation products. At 500–600 °C, it is the combustion of carbonaceous residue that releases a large amount of heat. All these results demonstrate that the prepared PVB sample has high thermal stability, and no substantial weight loss will occur at processing or operational temperature.

3.1.4 GPC. Fig. 3d shows the GPC profile and summary of self-made PVB, and tetrahydrofuran and polystyrene were selected as the mobile phase solvent and the standard sample respectively. The number average molecular weight (M_n) and weight average molecular weight (M_w) were determined as 38 678 and 61 487 g mol^{-1}, and the ratio of them (M_n/Mw) was 1.58972.

3.2 Modeling and parameters optimization by RSM

3.2.1 Analysis of variance (ANOVA). Twenty-nine experiments based on Tables 1 and 2 were carried out, and the results of the comprehensive score are also listed in Table 2. The quadratic regression model presented in terms of coded variables is obtained as follows:

$$Y = 91.20 - 0.16A + 1.80B + 1.58C - 3.46D - 1.39AB - 0.70AC + 0.27AD + 1.73BC + 0.19BD + 2.17CD - 3.29A^2 - 3.09B^2 - 4.89C^2 - 2.80D^2 \quad (8)$$

The results of ANOVA are shown in Table 3, which is used to evaluate the applicability of the model and judge the significance of each factor. As shown in Table 3, the model *F*-value of 73.09 and the *p*-value of < 0.0001 indicate that the model is significant. The lack of fit *F*-value of 5.50 and *p*-value of > 0.05 imply that lack of fit is quite low and not significant relative to the pure error. The high values of R^2 (0.9865) and adjusted R^2 (0.9730) indicate that the model fits well with the experimental data and has considerable compatibility.

Table 3 ANOVA for the quadratic model obtained by RSM

Source	Sum of squares	d*f*	Mean square	*F*-value	*p*-value	
Model	479.42	14	34.24	73.09	<0.0001	Significant
A	0.30	1	0.30	0.64	0.4365	
B	38.73	1	38.73	82.66	<0.0001	
C	29.93	1	29.93	63.88	<0.0001	
D	143.69	1	143.69	306.69	<0.0001	
AB	7.69	1	7.69	16.42	0.0012	
AC	1.94	1	1.94	4.14	0.0612	
AD	0.29	1	0.29	0.63	0.4411	
BC	12.03	1	12.03	25.69	0.0002	
BD	0.14	1	0.14	0.31	0.5883	
CD	18.87	1	18.87	40.27	<0.0001	
A^2	70.06	1	70.06	149.54	<0.0001	
B^2	61.93	1	61.93	132.19	<0.0001	
C^2	155.09	1	155.09	331.03	<0.0001	
D^2	50.99	1	50.99	108.83	<0.0001	
Residual	6.56	14	0.47			
Lack of fit	6.11	10	0.61	5.50	0.0574	Not significant
Pure error	0.44	4	0.11			
Cor total	485.98	28				

$R^2 = 0.9865$, Adj. $R^2 = 0.9730$, Adeq. precision = 30.28, C.V.% = 0.80%

Moreover, the *p*-value is an important criterion for determining the significance of each independent variable. Specifically, *p*-value > 0.05 is not significant; *p*-value < 0.05 is significant, and *p*-value < 0.01 is extremely significant. From Table 3, the *p*-values of independent variables *B*, *C*, and *D*, and interactions *AB*, *BC* and *CD* are all less than 0.05, indicating that they have significant effects on the quality of PVB resin, and other factors are not significant.

Adequate precision (AP) measures the signal-to-noise ratio, and a greater ratio value is desirable. The value of AP of this model is 30.28, which indicates that the model has a good predictive ability. The coefficient of variation (CV) is also known as the relative standard deviation and reflects the degree of dispersion of the data. The lower the CV value, the higher the reliability of the data. The low value of CV% (0.80%) shows that the experimental data is reliable.

Fig. 4 shows the comparison between the predicted *Y* values and the actual ones. From Fig. 4a, the points are arranged along a straight diagonal line; from Fig. 4b, the residuals are normally distributed and within the range of −3 to +3, indicating that the regression model is credible. In conclusion, the established quadratic polynomial model is reliable and can be used to optimize the PVB synthesis process.

3.2.2 Analysis of response surfaces. Based on the quadratic regression model, 3D response surface plots and 2D contour plots were constructed to describe the interaction effects between the independent variables, which can further help determine the optimal process conditions. Each response surface plot represents the change in response value with two variables when the other variables are at intermediate values, and the contour plot is a projection of a response surface. It can be seen in Table 3 that only the interactions *AB*, *BC* and *CD* have significant effects on the quality of PVB, and a detailed analysis of them is given as follows.

These 3D response surfaces and 2D contour plots show the interaction effects between PVA concentration and DES dosage (Fig. 5a and b), DES dosage and *n*-butanal dosage (Fig. 5c and d), *n*-butanal dosage and aging temperature (Fig. 5e and f) on the comprehensive score, respectively. From Fig. 5a and b, it can be found that as w_{PVA} and m_{DES}/m_{PVA} increased simultaneously, the comprehensive score first increased and then decreased. The comprehensive score was up to 90 when w_{PVA} was in the range of 5.5% ~8.5% and m_{DES}/m_{PVA} was in the range of 0.17–0.30. A similar trend was observed for the plots in Fig. 5c and d. As shown in Fig. 5c and d, the optimal regions for the two interacting variables were located in the middle area of the design, and the maximum value of the comprehensive score was achieved in the range of m_{DES}/m_{PVA} from 0.17 to 0.30, and m_{BA}/m_{PVA} from 0.72 to 0.85.

As shown in Fig. 5e and f, the 3D response surface plot is steepest and the associated contour plot shows a considerable curvature, indicating that the interaction between *n*-butanal dosage and aging temperature on the comprehensive score is the most significant, which is consistent with the *p*-value of CD (<0.0001). The comprehensive score first increased and then decreased with increasing *n*-butanal dosage, while it decreased as the aging temperature increased. The comprehensive score reached the highest value in the range of m_{BA}/m_{PVA} from 0.65 to 0.85, and T_{age} from 50 °C to 62 °C.

3.2.3 The optimal process conditions obtained by RSM model. The optimal process conditions for the synthesis of high quality PVB resins were obtained by solving the quadratic regression model using Design-Expert software. The optimal operation conditions were: $w_{PVA} = 6.9\%$, $m_{DES}/m_{PVA} = 0.25$, $m_{BA}/m_{PVA} = 0.81$ and $T_{age} = 57.3$ °C. The comprehensive score predicted at the optimal process conditions was 92.08, and the experimental validation under these conditions was 91.78, of which AD was 83.54% and d_p was 3.5 μm, indicating the good optimization performance of the RSM model.

3.3 Modeling and parameters optimization by ANN

3.3.1 Determination of the number of neurons in the hidden layer. The architecture of ANN was constructed based on

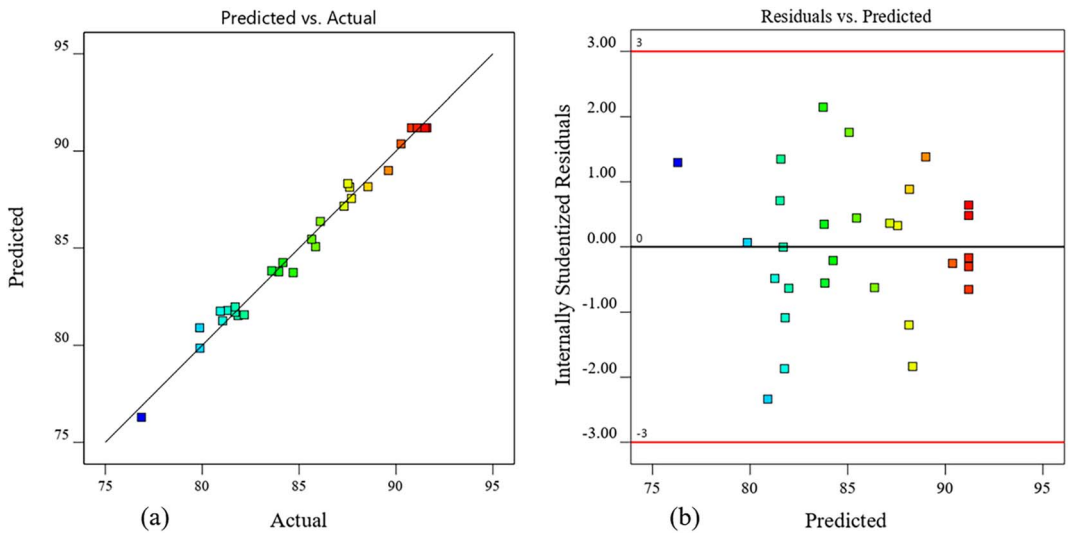

Fig. 4 (a) Plot of predicted *vs.* actual; (b) distribution of residuals *vs.* predicted.

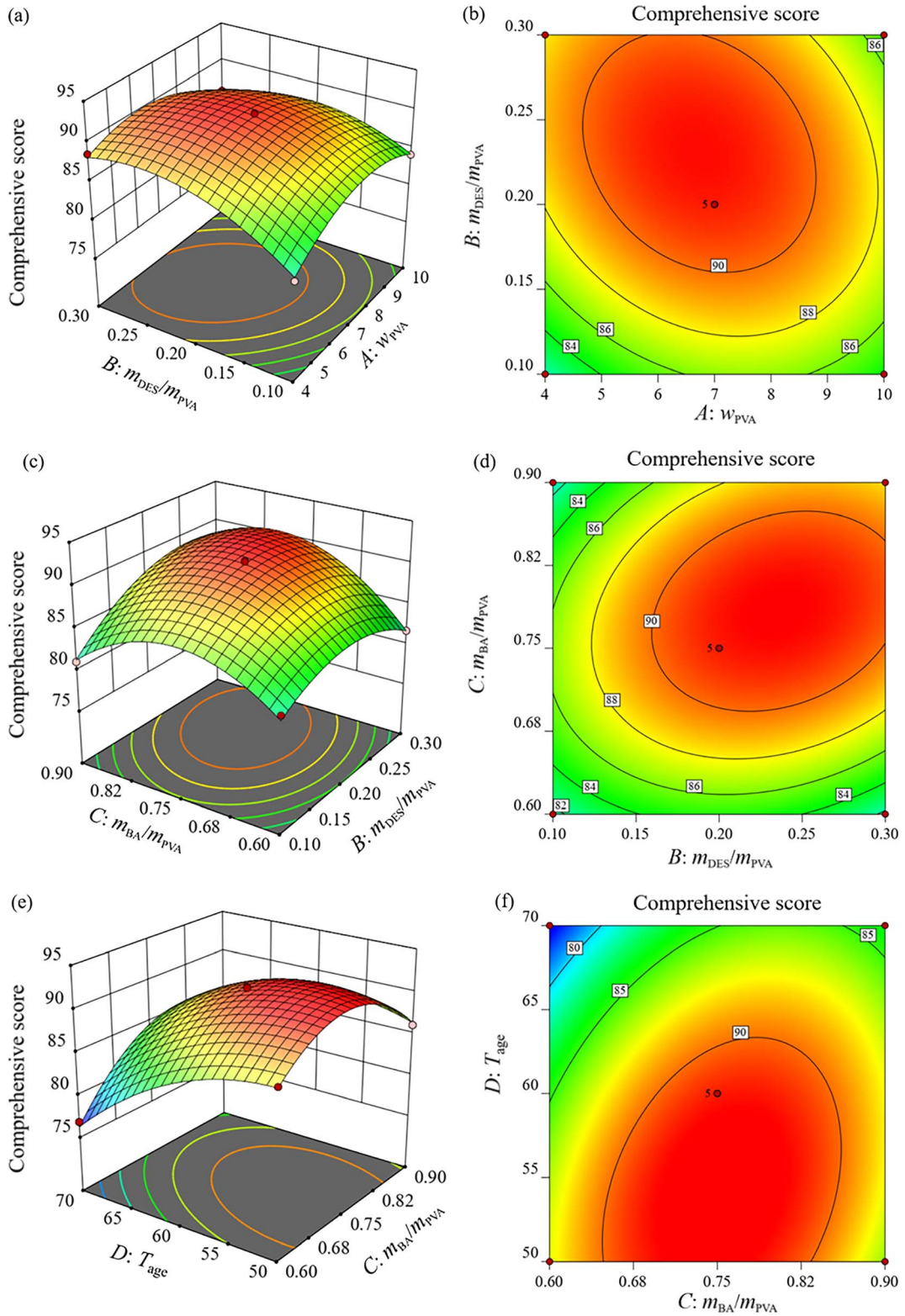

Fig. 5 Response surface plots and contour plots of interaction effects of AB (a and b), BC (c and d), and CD (e and f) on the comprehensive score.

the experimental data obtained from RSM (Table 2) and the relevant parameters described in section 2.8. According to eqn (4), the rough value of the number of neurons in the hidden layer was obtained to be 9. A relatively wide range was set from 4 to 14 to investigate the effect of the number of hidden layer neurons on the prediction performance of ANN model, and the results are shown in Fig. 6a. From Fig. 6a, the ANN structure with 8 neurons in the hidden layer presented the lowest MSE

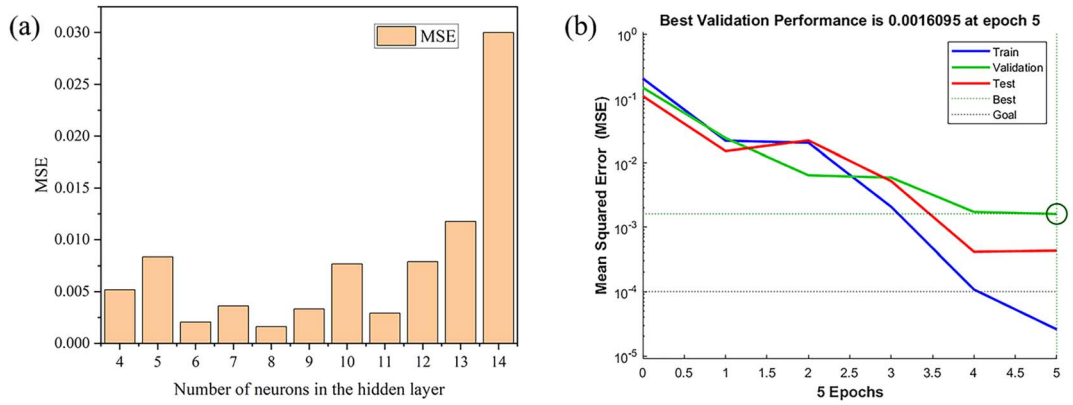

Fig. 6 ANN training. (a) Effect of the number of neurons on MSE value; (b) plots of MSE of training, validation and test verse to the epochs number.

value, and it was selected in ANN model in this work. Therefore, a three-layered BP ANN model with 4, 8, and 1 neurons in the input layer, hidden layer and output layer, respectively, was identified as the optimal model.

3.3.2 Analysis of ANN model results. Fig. 6b displays the relationship between the progression of training (TP), validation (VP) and test performance (TSP) during the simulation and the number of epochs. The MSE value dropped gradually as the number of epochs increased. The best validation performance was achieved in the 5th epoch, and the value of MSE was 0.0016095, indicating that the network is stable.

As the regression analysis of output and target are shown in Fig. 7a, the regression coefficients of training (0.99982), validation (0.9966), test (0.99985) and the network (training, testing and validation, 0.99809) are all greater than 0.99, which demonstrates a good fit. Fig. 7b shows the plot of the predicted comprehensive score *versus* the actual values of the training sample, and the predicted values are close to the actual values. The results of Fig. 7a and b indicate that the predictive capability of the ANN model is good, and the prediction result is reliable.

3.3.3 The optimal process conditions obtained by ANN model. The optimal process conditions obtained by the ANN model were: $w_{PVA} = 8.1\%$, $m_{DES}/m_{PVA} = 0.23$, $m_{BA}/m_{PVA} = 0.73$ and $T_{age} = 55.6$ °C, and the comprehensive score predicted at these conditions was 92.71. A validation experiment was carried out under the optimal process conditions, and the comprehensive score was calculated as 92.60, with AD of 81.35% and d_p of 3.0 μm, which confirmed the good predictive and optimization performance of the ANN model.

3.4 Comparison of RSM and ANN models

To verify the predictive performance of the models, validation experiments were performed under the optimal process conditions obtained by RSM and ANN models, which have been described in detail in the previous section. The values of AD, d_p and the comprehensive score of PVB products are summarized in Table 4, and the SEM images of PVB obtained by RSM and

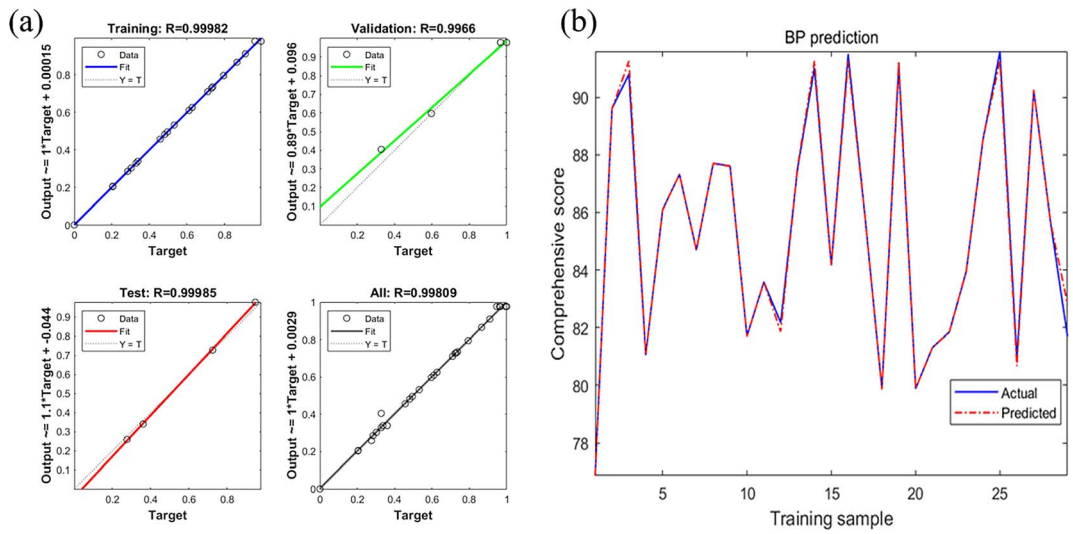

Fig. 7 (a) Regression plot of output *vs.* target; (b) actual and predicted comprehensive score.

Table 4 Comparison of RSM and ANN models

Model	R^2	RMSE	AAD (%)	AD (%)	d_p (μm)	Comprehensive score	
						Actual	Predicted
RSM	0.9865	0.4754	0.45	83.54	3.5	91.78	92.08
ANN	0.9962	0.2551	0.13	81.35	3.0	92.60	92.71

ANN are shown in Fig. 8a and b, respectively. As shown in Table 4, the PVB product obtained by RSM has slightly higher AD and d_p values than that of PVB obtained by ANN. The differences mainly because DES dosage, *n*-butanal dosage, and T_{age} in the optimal process conditions of RSM all exceeded those of ANN, which accelerated the acetal reaction rate and increased AD. However, the excessively fast reaction rate and higher temperatures resulted in the product molecules not being dispersed in time and sticking together, so the PVB particles were larger. Compared with the RSM model, the value of the comprehensive score obtained by the ANN model is higher and much closer to its predicted value, indicating that the optimal process condition obtained from ANN has better reliability and accuracy.

The performance of the RSM and ANN models was further compared based on three statistical indicators (R^2, RMSE, and AAD%). As shown in Table 4, both models have R^2 values close to 1 and very low RSME and AAD% values. However, ANN has a higher R^2 value and lower RMSE and AAD% values. Therefore, it can be concluded that both RSM and ANN are efficient tools for optimizing the synthesis process of PVB, and the optimization performance and prediction accuracy of ANN model is better than RSM model.

3.5 Recycling experiments

The reusability of the catalyst is an important factor for its large-scale industrial application. Based on the above results, the recycling experiments were conducted based on the optimal process conditions obtained from the ANN model. After the aging reaction, PVB particles were separated by centrifugation and the mother liquor was collected. The content of DES and *n*-butanal remaining in the solution was measured through acid–base titration and UV spectrophotometer, respectively. The mother liquor was used as the raw material for the recycling experiment, and the required amounts of DES, water, *n*-butanal and SDS were carefully calculated and supplemented, and the experimental operations were performed as previously described. The detailed experimental parameters and results are shown in Table 5, and the SEM images are shown in Fig. 8c and d. As shown in Table 5 and Fig. 8c, the AD and d_p values of PVB product in the recycling experiment (*R*1) were similar to those in the basic experiment (Fig. 8b), and the comprehensive score reached 92.49, indicating good reusability of DES (BAC–PTSA) for the

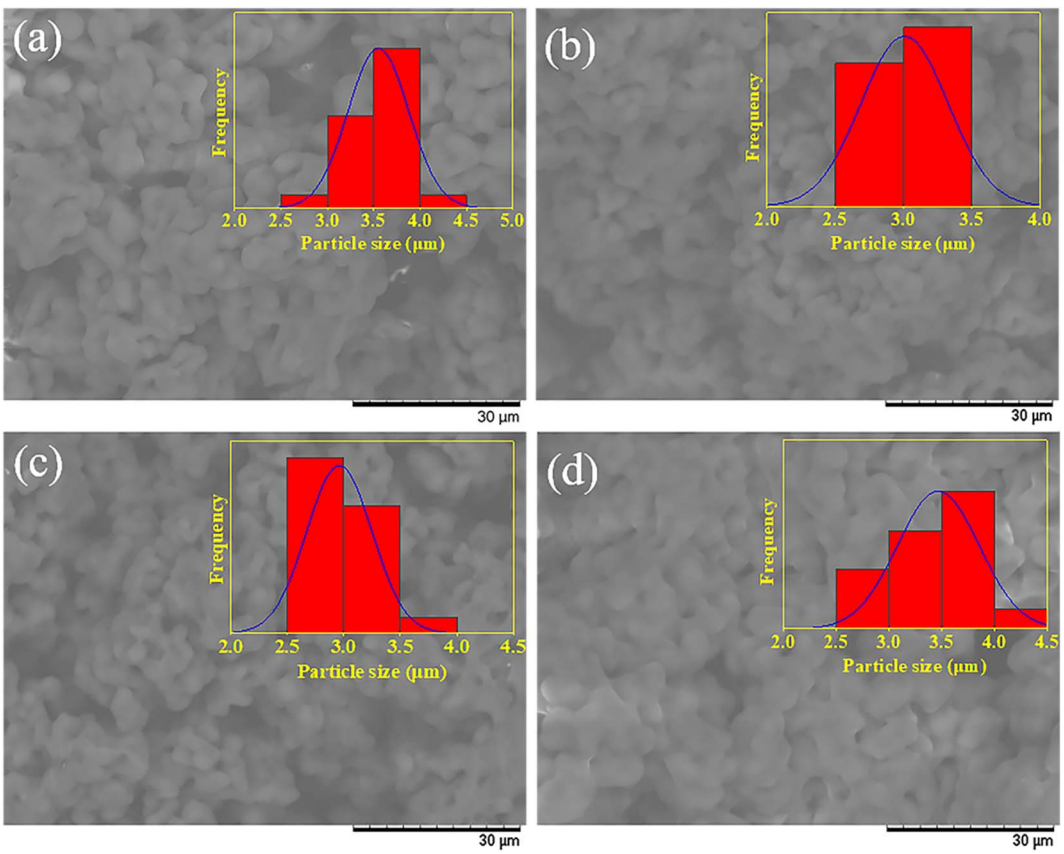

Fig. 8 SEM images of PVB samples obtained by RSM (a), ANN (b); recycling experiments: *R*1 (c) and *R*2 (d).

Table 5 Comparison of the amount of main substances added in the basic and recycling experiments

	Water (m_{water}/m_{PVA})	DES (m_{DES}/m_{PVA})	*n*-Butanal (m_{BA}/m_{PVA})	SDS (m_{SDS}/m_{PVA})	AD (%)	d_p (μm)	Comprehensive score
Basic	12.4	0.230	0.73	0.01	81.35	3.0	92.60
*R*1	1.4	0.026	0.61	0.003	81.20	3.0	92.49
*R*2	1.4	0	0.61	0	80.41	3.5	89.35

synthesis reaction of PVB. A contrast recycling experiment (*R*2) was carried out in which only water and *n*-butanal were supplemented to the mother liquor, while DES and SDS were not supplemented. As shown in Table 5 and Fig. 8d, PVB products obtained by *R*2 had lower AD and larger d_p than those of the basic experiment and *R*1. This may be because the loss of DES slowed down the reaction rate, so the AD of PVB obtained in the same reaction time was lower. In addition, the loss of both DES and SDS led to a poor dispersion effect, so the particle size of PVB was large. Qualified PVB products could be obtained by supplementing a small amount of lost raw material, demonstrating the feasibility of the recycling technology in PVB practical production.

4. Conclusions

In this work, DES (BAC–PTSA) was prepared and selected as the catalyst for the synthesis of PVB. RSM and ANN were applied to investigate the effects of PVA concentration, DES dosage, *n*-butanal dosage and aging temperature on the quality of PVB resin, and to predict the optimal synthesis process conditions of PVB. The obtained results showed that both RSM and ANN were efficient tools for optimizing the synthesis process of PVB, and ANN is a better and more precise optimization tool than RSM. The optimal process conditions predicted by ANN were $w_{PVA} = 8.1\%$, $m_{DES}/m_{PVA} = 0.23$, $m_{BA}/m_{PVA} = 0.73$ and $T_{age} = 55.6$ °C with the predicted comprehensive score of 92.71, which was validated as 92.60. Moreover, PVB products obtained in the recycling experiment had similar AD values and particle morphologies to those of the basic experiment. It can be concluded that the DES used in this work exhibited good catalytic and dispersion properties, as well as excellent reusability, in which not only the amount of SDS but also the discharge of wastewater was reduced, so it has great application potential in PVB industrial production.

Author contributions

Wenwen Luan: conceptualization, validation, data curation, writing – original draft, writing – review & editing; Li Sun: resources, software; Zuoxiang Zeng: formal analysis, validation, writing – review & editing; Weilan Xue: conceptualization, supervision.

Conflicts of interest

There are no conflicts to declare.

References

1 L. Calucci, S. Pizzanelli, A. Mandoli, A. Birczynski, Z. T. Lalowicz, C. De Monte, L. Ricci and S. Bronco, *Polymers*, 2021, **13**, 2686.
2 J. C. Hoepfner, M. R. Loos and S. H. Pezzin, *J. Appl. Polym. Sci.*, 2019, **136**, 48146.
3 B. Y. Zhou, X. Y. Lin, K. Wang and G. S. Luo, *Ind. Eng. Chem. Res.*, 2017, **56**, 14463–14470.
4 B. Guner, Y. E. Bulbul and N. Dilsiz, *J. Taiwan Inst. Chem. Eng.*, 2022, **132**, 104136.
5 J. Xu, Y. Li, D. Ge, B. Liu and M. Zhu, *Int. J. Impact Eng.*, 2011, **38**, 106–114.
6 X. Zhang, H. Hao, Y. Shi and J. Cui, *Constr. Build. Mater.*, 2015, **93**, 404–415.
7 X. Huang, Y. Lin and G. Fang, *Solar Energy*, 2018, **161**, 187–193.
8 N. G. Dhere, K. Agroui, B. Koll, G. Collins, M. Salama, A. Hadj Arab, A. Belghachi, N. Doulache and M. W. Khemici, *Presented in Part at the Reliability of Photovoltaic Cells, Modules, Components, and Systems*, 2008.
9 H. Yao, X. Zhang, L. Shen and N. Bao, *Prog. Org. Coat.*, 2021, **158**, 106382.
10 Z. Ma, M. Sun, A. Li, G. Zhu and Y. Zhang, *Prog. Org. Coat.*, 2020, **144**, 105662.
11 L. Xiong, J. Liu, M. Yu and S. Li, *Corros. Sci.*, 2019, **146**, 70–79.
12 W.-Z. Lang, J.-P. Shen, Y.-X. Zhang, Y.-H. Yu, Y.-J. Guo and C.-X. Liu, *J. Membr. Sci.*, 2013, **430**, 1–10.
13 X. Ma, Q. Sun, Y. Su, Y. Wang and Z. Jiang, *Sep. Purif. Technol.*, 2007, **54**, 220–226.
14 H. Azad, M. Mohsennia, C. Cheng and A. Amini, *Chem. Eng. J.*, 2022, **435**, 134849.
15 B. Yang, R. Liu, J. Huang and H. Sun, *Ind. Eng. Chem. Res.*, 2013, **52**, 7425–7431.
16 X. Lin, S. Yan, B. Zhou, K. Wang, J. Zhang and G. Luo, *Green Chem.*, 2017, **19**, 2155–2163.
17 M. D. Fernández, M. J. Fernández and P. Hoces, *J. Appl. Polym. Sci.*, 2006, **102**, 5007–5017.
18 M. Nasrollahzadeh, Z. Nezafat, F. Momenbeik and Y. Orooji, *J. Mol. Liq.*, 2022, **345**, 117811.
19 Y. Pei, Y. Zhang, J. Ma, M. Fan, S. Zhang and J. Wang, *Mater. Today Nano*, 2022, **17**, 100159.
20 C. G. Yoo, Y. Pu and A. J. Ragauskas, *Curr. Opin. Green Sustainable Chem.*, 2017, **5**, 5–11.
21 X.-X. Qin and Z.-L. Cheng, *Chin. Chem. Lett.*, 2016, **27**, 145–148.

22 A. Romero, A. Santos, J. Tojo and A. Rodriguez, *J. Hazard. Mater.*, 2008, **151**, 268–273.
23 K. Li, X. Chen, W. Xue, Z. Zeng and S. Jiang, *Int. J. Chem. Kinet.*, 2019, **51**, 329–336.
24 A. Hayyan, M. A. Hashim, M. Hayyan, F. S. Mjalli and I. M. AlNashef, *J. Cleaner Prod.*, 2014, **65**, 246–251.
25 S. Jiang, Z. Zeng, W. Xue, W. Zhang and Z. Zhou, *Korean J. Chem. Eng.*, 2020, **37**, 1482–1489.
26 K. Li, W. Xue, Z. Zeng and X. Shi, *Can. J. Chem. Eng.*, 2018, **97**, 1144–1151.
27 M. H. Shafie, R. Yusof and C.-Y. Gan, *J. Mol. Liq.*, 2019, **288**, 111081–111086.
28 Y. Guo, L. Tang, W. Xue and Z. Zeng, *Int. J. Chem. Kinet.*, 2021, **53**, 1241–1252.
29 M. K. Miraki, J. A. Mehraban, E. Yazdani and A. Heydari, *J. Mol. Liq.*, 2017, **234**, 129–132.
30 L. Tang, Y. Guo, J. Xu, Z. Zeng and W. Xue, *Braz. J. Chem. Eng.*, 2022, **39**, 715–726.
31 H. Wang, W. Luan, L. Sun, Z. Zeng, W. Xue and Y. Bai, *Chem. Eng. Res. Des.*, 2022, **184**, 291–302.
32 Q. Liu, W. Sun, T. Yuan, S. B. Liang, F. Peng and C. L. Yao, *Carbohydr. Polym.*, 2021, **272**, 118514.
33 A. Brandao, S. Rosoiu, R. Costa, A. F. Silva, L. Anicai, M. Enachescu and C. M. Pereira, *Nanomaterials*, 2021, **12**, 99–121.
34 A. Abo-Hamad, M. Hayyan, M. A. AlSaadi and M. A. Hashim, *Chem. Eng. J.*, 2015, **273**, 551–567.
35 N. Asanjarani, M. Bagtash and J. Zolgharnein, *J. Chemom.*, 2020, **34**, e3283.
36 S. M. Huang, C. H. Kuo, C. A. Chen, Y. C. Liu and C. J. Shieh, *Ultrason. Sonochem.*, 2017, **36**, 112–122.
37 F. Wang, L. Chen, S. Jiang, J. He, X. Zhang, J. Peng, Q. Xu and R. Li, *J. Liposome Res.*, 2014, **24**, 171–181.
38 L. Zhao, Q. Li, X. Xu, W. Kong, X. Li, Y. Su, Q. Yue and B. Gao, *Chem. Eng. J.*, 2016, **287**, 537–544.
39 S. N. Ayyubi, A. Purbasari and Kusmiyati, *Mater. Today: Proc.*, 2022, **63**, S78–S83.
40 S. Rathee and A. Kamboj, *J. Liposome Res.*, 2018, **28**, 161–172.
41 Y. Zhang, L. Zhou, Z. Hu, Z. Yu, S. Hao, Z. Lei and Y. Xie, *Energies*, 2018, **11**, 1896.
42 M. Yue and S. Li, *AJRCOS*, 2022, **13**, 1–12.
43 J. Gao, P. Chongfuangprinya, Y. Z. Ye and B. Yang, *IEEE, Electr. Network*, 2020.
44 Y. Lecun, L. Bottou, Y. Bengio and P. Haffner, *Proc. IEEE*, 1998, **86**, 2278–2324.
45 J. Gao, D. Chakraborty, H. Tembine and O. Olaleye, *A. Int Speech Commun*, Graz, Austria, 2019.
46 M. A. Khan, H. Tembine and A. V. Vasilakos, *IEEE Wireless Commun.*, 2012, **19**, 50–56.
47 F. Shi, J. Gao and X. Huang, *Int. J. Distrib. Sens. Netw.*, 2016, **12**, 1–12.
48 J. Gao and H. Tembine, *IEEE Trans. Intell. Transport. Syst.*, 2019, **20**, 507–521.
49 W. Haonan and C. Yijia, *AJRCOS*, 2022, **14**, 22–37.
50 Y. Si and B. He, *AJRCOS*, 2022, **14**, 1–7.
51 F. Xindi and S. Li, *JERR*, 2022, **23**, 26–36.
52 G. Petroli, I. Dalmolin and C. Z. Brusamarello, *Chem. Thermodyn. Therm. Anal.*, 2022, **6**, 100048.
53 C. Wang and C. Li, *AJRCOS*, 2021, **11**, 8–16.
54 J. H. Haido, *Structures*, 2022, **38**, 1191–1209.
55 M. R. Sabour and A. Amiri, *Waste Manag.*, 2017, **65**, 54–62.
56 I. G. Ezemagu, M. I. Ejimofor, M. C. Menkiti and C. C. Nwobi-Okoye, *S. Afr. J. Chem. Eng.*, 2021, **35**, 78–88.
57 A. L. Toppo, S. Dhagat and S. E. Jujjavarapu, *Prep. Biochem. Biotechnol.*, 2022, **53**, 195–206.
58 W. Luan, J. Xu, Z. Zeng, W. Xue and Y. Bai, *Can. J. Chem. Eng.*, 2023, **1**, 1–14.
59 W. Luan, C. Wang, Z. Zeng, W. Xue, F. Liang and Y. Bai, *J. Mol. Liq.*, 2021, **336**, 116864.
60 W. Luan, C. Wang, Z. Zeng, W. Xue, X. He and Y. Bai, *Korean J. Chem. Eng.*, 2021, **38**, 1810–1817.
61 L. Tong, P. Bénard, Y. Zong, R. Chahine, K. Liu and J. Xiao, *Energy and AI*, 2021, **5**, 10075.
62 F. Geyikçi, E. Kılıç, S. Çoruh and S. Elevli, *Chem. Eng. J.*, 2012, **183**, 53–59.
63 E. Betiku and S. O. Ajala, *Ind. Crops Prod.*, 2014, **53**, 314–322.
64 Q.-Q. Yang, R.-Y. Gan, D. Zhang, Y.-Y. Ge, L.-Z. Cheng and H. Corke, *LWT–Food Sci. Technol.*, 2019, **114**, 108321.
65 E. Corroyer, M.-C. Brochier-Salon, D. Chaussy, S. Wery and M. N. Belgacem, *Int. J. Polym. Anal. Charact.*, 2013, **18**, 346–357.
66 G. C. Kingston and H. K. Yuen, *Thermochim. Acta*, 1987, **116**, 317–327.
67 X. Li, B. Shen, J. Chen, J. Yang and J. Yang, *Henan Sci.*, 1994, **12**, 111–115.
68 C. Wang, W. Luan, Z. Zeng, X. He, Z. Liu and J. H. Wang, *Polym. Bull.*, 2022, DOI: **10.1007/s00289-022-04366-0**.